Curvature effects on the surface thickness and tension at the free interface of ^{4}He systems

Leszek Szybisz[1,2,*] and Ignacio Urrutia[1,†]
[1]*Laboratorio TANDAR, Departamento de Física, Comisión Nacional de Energía Atómica, Av. del Libertador 8250, RA-1429 Buenos Aires, Argentina*
[2]*Departamento de Física, Facultad de Ciencias Exactas y Naturales, Universidad de Buenos Aires, Ciudad Universitaria, RA-1428 Buenos Aires, Argentina*
(Received 31 March 2003; published 19 August 2003)

The thickness W and the surface energy σ_A at the free interface of superfluid ^{4}He are studied. Results of calculations carried out using density functionals for cylindrical and spherical systems are presented in a unified way, including a comparison with the behavior of planar slabs. It is found that for large species W is independent of the geometry. The obtained values of W are compared with prior theoretical results and experimental data. Experimental data favor results evaluated by adopting finite range approaches. The behavior of σ_A and $W\sigma_A$ exhibits overshoots similar to that found previously for the central density, and the trend of these observables towards their asymptotic values is examined.

DOI: 10.1103/PhysRevB.68.054518 PACS number(s): 61.20.−p, 68.03.Cd

I. INTRODUCTION

The understanding of the density profiles in the surface region of a quantum fluid such as ^{4}He has long been considered a very important basic problem.[1–3] At the liquid-vapor interface, the density profile of ^{4}He changes continuously from liquid density ρ_ℓ to vapor density ρ_v over a distance of some Angström. In the case of a liquid-vacuum interface at $T=0$ K, ρ_ℓ falls monotonically to $\rho_v=0$. The width W of a surface is defined as the distance in which the density decreases from $0.9\rho_\ell$ to $0.1\rho_\ell$. A glance at recent literature reveals several works addressing the question of the thickness of the free interface,[4–7] indicating the continuous interest in this area of theoretical and experimental research. The surface tension at the free interface has been also investigated for a long time.[1,5,8–12] A list of results for the surface thickness and tension determined up to the middle of 1987 is given by Osborne in Table 1 of Ref. 2.

In the systematic study of free planar ^{4}He films at $T=0$ K we have, among other issues, discussed features of the surface thickness.[5] There, our own results for W evaluated using several density-functional (DF) approaches are compared with values obtained from Monte Carlo simulations by Vallés and Schmidt[12] and experimental data of Lurio *et al.*[3] From Fig. 4 in Ref. 5 one can realize that the size of the experimental error bar was too large to disregard any of the applied DF approaches. After that paper had been published, other theoretical and experimental results for this quantity have appeared. Evaluations of W for free planar slabs and droplets utilizing a variational Monte Carlo approach with shadow wave functions (SWF) with a glue term (glue-SWF) were published by Galli and Reatto.[6] On the other hand, a different measurement of W using x-ray reflectivity was reported by Penanen *et al.*[7] These data superseded that previously obtained at the same laboratory.[3] To complete the survey of investigations about the surface thickness of superfluid helium droplets, one should mention the calculation of Stringari and Treiner[13] and the comprehensive experimental and theoretical study of Harms, Toennies, and Dalfovo.[4]

The foregone summary indicates that there is an important piece of information about the free surface thickness of planar and spherical superfluid ^{4}He systems that is missing. Although in recent years there has been a renewal of interest for examining cylindrical species,[14–20] hitherto, there has been no study undertaking the problem of exploring features of W in the case of such geometry, to our best knowledge.

We have explored the evolution of the surface energy at the liquid-vacuum interface of planar slabs as a function of their size in Ref. 5. However, as far as we know, there has been no work devoted to studying this property in the case of systems with curved geometries. Therefore, such an analysis becomes an interesting problem by its own right.

In view of the situation described above, the aim of this work is to study systematically the interface thickness and the surface tension of liquid ^{4}He with cylindrical and spherical shapes, making a connection to the case of planar slabs. Although the spherical systems are energetically favored against free cylinders and slabs an analysis of the overall picture presents instructive features. The width at the liquid-vacuum interface of free systems is compared with experimental data and with theoretical results obtained for stable planar films of ^{4}He adsorbed onto the lightest alkali metals. The theoretical tools are outlined in Sec. II. In Sec. III we search for the size at which the systems reach its asymptotic global behavior. The discussion of the pattern exhibited by the width and tension at the surface may be found in Sec. IV, where the results are presented in a unified way allowing a direct comparison of data obtained for different geometries. Section V is devoted to a summary.

II. THEORETICAL FRAMEWORK

The calculations performed in the present work were carried out using DF approaches, which have proven to be successful tools for treating this kind of quantum many-body problem. In such a theory the ground-state energy, $E_{\rm gs}$, of an interacting N-body system of ^{4}He atoms, confined by an adsorbate-substrate potential $U_{\rm sub}(\mathbf{r})$, may be written as

$$E_{\rm gs}=\int d\mathbf{r}\rho(\mathbf{r})\mathcal{H}[\rho,\boldsymbol{\nabla}\rho]+\int d\mathbf{r}\rho(\mathbf{r})U_{\rm sub}(\mathbf{r})$$
$$=-\frac{\hbar^2}{2m}\int d\mathbf{r}\sqrt{\rho(\mathbf{r})}\boldsymbol{\nabla}^2\sqrt{\rho(\mathbf{r})}+\int d\mathbf{r}\rho(\mathbf{r})e_{sc}(\mathbf{r})$$
$$+\int d\mathbf{r}\rho(\mathbf{r})U_{\rm sub}(\mathbf{r}), \quad (2.1)$$

where $\rho(\mathbf{r})$ is the one-body density. The first term on the right-hand side is the quantum kinetic energy of the helium particles of mass m. The second term represents the interaction between the particles of the system, where $e_{sc}(\mathbf{r})$ is the self-correlation energy per particle depending on the DF approach. The last term is the interaction with the external field.

The density profile $\rho(\mathbf{r})$ is determined from the Euler-Lagrange equation derived from the condition

$$\frac{\delta\Omega}{\delta\rho(\mathbf{r})}=\frac{\delta\{E_{\rm gs}[\rho,\boldsymbol{\nabla}\rho]-\mu N\}}{\delta\rho(\mathbf{r})}=0. \quad (2.2)$$

Here μ is the chemical potential, N the number of particles,

$$N=\int d\mathbf{r}\rho(\mathbf{r}), \quad (2.3)$$

and Ω the grand thermodynamic potential. The variation of Eq. (2.2) leads to a Hartree-like equation for the square root of the one-body density

$$\left[-\frac{\hbar^2}{2m}\boldsymbol{\nabla}^2+V_H(\mathbf{r})+U_{\rm sub}(\mathbf{r})\right]\sqrt{\rho(\mathbf{r})}=\mu\sqrt{\rho(\mathbf{r})}, \quad (2.4)$$

which also determines μ. Here $V_H(\mathbf{r})$ is a Hartree mean-field potential given by the first functional derivative of the total correlation energy $E_{sc}[\rho]$,

$$V_H(\mathbf{r})=\frac{\delta E_{sc}[\rho,\boldsymbol{\nabla}\rho]}{\delta\rho(\mathbf{r})}=\frac{\delta}{\delta\rho(\mathbf{r})}\int d\mathbf{r}'\rho(\mathbf{r}')e_{sc}(\mathbf{r}')$$
$$=\left[\frac{\partial}{\partial\rho(\mathbf{r})}-\boldsymbol{\nabla}\frac{\partial}{\partial\boldsymbol{\nabla}\rho(\mathbf{r})}\right]\int d\mathbf{r}'\rho(\mathbf{r}')e_{sc}(\mathbf{r}'). \quad (2.5)$$

Two different DFs were used, namely, the Skyrme-type ''zero-range'' version suggested in Refs. 13 and 21, and the nonlocal-density functional (NLDF) proposed in Ref. 22. For each DF an expression for $V_H(r)$ should be derived.

A. Zero-range density functional

The simplest DF successfully employed to interpret properties of ^{4}He systems is a zero-range correlation proposed by Stringari and Treiner.[13,21] It has been inspired in Skyrme-type functionals extensively used to describe properties of atomic nuclei.[23,24] The explicit form of this correlation energy per particle is

$$e_{sc}^{\rm Sky}(\mathbf{r})=\frac{b_4}{2}\rho(\mathbf{r})+\frac{c_4}{2}\rho^{\gamma_4+1}(\mathbf{r})+d_4\frac{1}{\rho(\mathbf{r})}|\nabla\rho(\mathbf{r})|^2. \quad (2.6)$$

TABLE I. Bulk observables for liquid ^{4}He at $T=0$ and the calculated parameters ε_ℓ and a_c. PW stands for results obtained in the present work.

Observable	Data		Reference
e_B (K)	-7.15		21
ρ_0 (Å^{-3})	0.021836		21
$\mathcal{K}$ (K)	27.2		21
$\sigma_{\rm exp}$ (K/Å^2)	0.274 ± 0.003		8
	0.257 ± 0.001		9
	0.272 ± 0.002		10
Parameter	**Value**	**Theory**	**Reference**
ε_ℓ (K/Å)	1.237	Skyrme DF	PW
ε_ℓ (K/Å)	0.882	OP NLDF	PW
a_c (K)	10.45	Skyrme DF	13
a_c (K)	10.90		21
a_c (K)	10.86		PW
a_c (K)	8.58	OP NLDF	PW
$(\pi\rho_0/48)^{1/3}a_c/\varepsilon_\ell$	0.99	Skyrme DF	PW
$(\pi\rho_0/48)^{1/3}a_c/\varepsilon_\ell$	1.10	OP NLDF	PW
$(\pi\rho_0/48)^{1/3}a_c/\varepsilon_\ell$	1.00	DM	Eq. (4.38); PW

The phenomenological parameters b_4, c_4, γ_4, and d_4 have been fixed in Ref. 13 so as to reproduce the known observables of the bulk liquid at equilibrium. The data of these saturation quantities (where $P=0$), i.e., the equilibrium density ρ_0, the minimum energy per particle e_B, the compressibility $\mathcal{K}$, and the surface tension σ_∞ of a semi-infinite ^{4}He system, are listed in Table I. Experimental values are correctly reproduced by the set

$$b_4=-8.88810\times10^2 \ \text{K Å}^3,$$
$$c_4=1.045\,54\times10^7 \ \text{K Å}^{3(\gamma_4+1)},$$
$$\gamma_4=2.8,$$
$$d_4=2.383\times10^3 \ \text{K Å}^5. \quad (2.7)$$

B. Orsay-Paris nonlocal-density functional

Currently, in the literature one may find a few NLDF approaches. The Orsay-Paris (OP) version (OP-NLDF) developed by Dupont-Roc *et al.*[22] treats correctly the long-range part of the helium-helium interaction and provides a reasonable description of correlations. The most elaborate version has been formulated by the Orsay-Trento (OT) collaboration.[25] However, the OP-NLDF is sufficient to reproduce properties of nonlayered samples such as free or weakly confined systems. This functional reads

$$e_{sc}^{\rm OP}(\mathbf{r})=\frac{1}{2}\int d\mathbf{r}'\rho(\mathbf{r}')V_l^{\rm OP}(|\mathbf{r}-\mathbf{r}'|)+\frac{c_4}{2}[\overline{\rho}(\mathbf{r})]^{\gamma_4+1}. \quad (2.8)$$

In this case the two-body interaction, $V_l^{\mathrm{OP}}(|\mathbf{r}-\mathbf{r}'|)$, was taken as the ^{4}He-^{4}He Lennard-Jones (LJ) potential screened in a simple way at distances shorter than a characteristic distance h_{OP},

$$V_l^{\mathrm{OP}}(r)=\begin{cases} 4\epsilon_{\mathrm{LJ}}\left[\left(\dfrac{\sigma_{\mathrm{LJ}}}{r}\right)^{12}-\left(\dfrac{\sigma_{\mathrm{LJ}}}{r}\right)^{6}\right] & \text{if } r\geqslant h_{\mathrm{OP}}, \\ V_l^{\mathrm{OP}}(h_{\mathrm{OP}})\left(\dfrac{r}{h_{\mathrm{OP}}}\right)^4 & \text{if } r<h_{\mathrm{OP}}, \end{cases} \tag{2.9}$$

with the standard de Boer and Michels parameters,[26] namely, well depth $\epsilon_{\mathrm{LJ}}=10.22$ K and hard-core radius $\sigma_{\mathrm{LJ}}=2.556$ Å. In order to recover the correct results for bulk liquid, the screening distance h_{OP} was adjusted so that the integral of $V_l^{\mathrm{OP}}(r)$ over the whole three-dimensional space is equal to the value of b_4 given by Eq. (2.7),

$$b_4=\int d\mathbf{r}V_l^{\mathrm{OP}}(r)=\frac{32\pi}{21}\sigma_{\mathrm{LJ}}^3\epsilon_{\mathrm{LJ}}\left[\frac{8}{3}\left(\frac{\sigma_{\mathrm{LJ}}}{h_{\mathrm{OP}}}\right)^9-5\left(\frac{\sigma_{\mathrm{LJ}}}{h_{\mathrm{OP}}}\right)^3\right]. \tag{2.10}$$

This procedure led to $h_{\mathrm{OP}}=2.376\,728$ Å.

The $\overline{\rho}(\mathbf{r})$ is the ''coarse-grained density'' defined as the straight average of $\rho(\mathbf{r})$ over a sphere centered at $\mathbf{r}$ and with a radius equal to the screening distance h_{OP},

$$\overline{\rho}(\mathbf{r})=\int d\mathbf{r}'\rho(\mathbf{r}')\mathcal{W}(|\mathbf{r}-\mathbf{r}'|), \tag{2.11}$$

where $\mathcal{W}(|\mathbf{r}-\mathbf{r}'|)$ is taken as the normalized step function

$$\mathcal{W}(|\mathbf{r}-\mathbf{r}'|)=\frac{3}{4\pi h_{\mathrm{OP}}^3}\Theta(h_{\mathrm{OP}}-|\mathbf{r}-\mathbf{r}'|) =\begin{cases} \dfrac{3}{4\pi h_{\mathrm{OP}}^3} & \text{if } |\mathbf{r}-\mathbf{r}'|\leqslant h_{\mathrm{OP}}, \\ 0 & \text{if } |\mathbf{r}-\mathbf{r}'|>h_{\mathrm{OP}}. \end{cases} \tag{2.12}$$

C. Hartree-like equation

In the case of curved geometries Eq. (2.4) takes the form

$$-\frac{\hbar^2}{2m}\left(\frac{d^2}{dr^2}+\frac{D-1}{r}\frac{d}{dr}\right)\sqrt{\rho(r)}+[V_H(r)+U_{\mathrm{sub}}(r)]\sqrt{\rho(r)} =\mu\sqrt{\rho(r)}, \tag{2.13}$$

with $D=2$ for cylindrical systems and $D=3$ for spherical ones. The equation for planar systems is obtained by setting $D=1$ and assuming that r represents the coordinate perpendicular to the plane of symmetry (usually denoted z). The Hartree potential derived by applying Eq. (2.5) to the Skyrme DF reads

$$V_H^{\mathrm{Sky}}(r)=b_4\rho(r)+\frac{\gamma_4+2}{2}c_4\rho^{\gamma_4+1}(r) -2d_4\left(\frac{d^2}{dr^2}+\frac{D-1}{r}\frac{d}{dr}\right)\rho(r). \tag{2.14}$$

The expression for $V_H(r)$ derived in the OP-NLDF approach for cylindrical systems is given in the Appendix of Ref. 18. The corresponding one for spherical systems is provided in Appendix A of the present work. It is worthwhile to notice that we expressed this quantity in a rather simple compact form similar to Eq. (2.16) written in Ref. 27 for planar films instead of adopting the expansion in terms of Legendre polynomials proposed in Ref. 28. The latter procedure is more appropriate for studying excitations of a given system. We mainly report results for curved geometries obtained by setting $U_{\mathrm{sub}}(r)\equiv 0$.

In the case of cylindrical symmetry Eq. (2.13) is solved for a fixed number of particles per unit length L,

$$n_\lambda=N/L=2\pi\int_0^\infty rdr\rho(r), \tag{2.15}$$

while for helium spheres the constraint is directly the number of particles,

$$N=4\pi\int_0^\infty r^2dr\rho(r). \tag{2.16}$$

Typical density profiles are displayed in Fig. 2 of Ref. 18 for cylinders and in Fig. 1 of Ref. 13 for spheres.

We first test whether the size of the considered systems of liquid ^{4}He is large enough to expect asymptotic behaviors. Next, we focus our attention on the surface energy and the width of the interface.

III. ASYMPTOTIC GLOBAL BEHAVIOR OF THE SYSTEMS

In the case of spherical systems, it has become customary to define for each moment $\langle r^k\rangle$ an equivalent uniform radius R_k. This quantity is equal to the radius of a uniformly occupied sphere (of density ρ_u) with the same momentum of order k given by the true density distribution. It is possible to extend this idea to the cylindrical geometry. So, in general, an equivalent uniform radius R_k associated to a momentum r^k given by

$$\langle r_u^k\rangle_D=\frac{2^{D-1}\pi L^{3-D}\int_0^{R_k}drr^{k+D-1}\rho_u}{2^{D-1}\pi L^{3-D}\int_0^{R_k}drr^{D-1}\rho_u} =\frac{\int_0^{R_k}drr^{k+D-1}\rho_u}{\int_0^{R_k}drr^{D-1}\rho_u}=\frac{D}{k+D}R_k^k \tag{3.1}$$

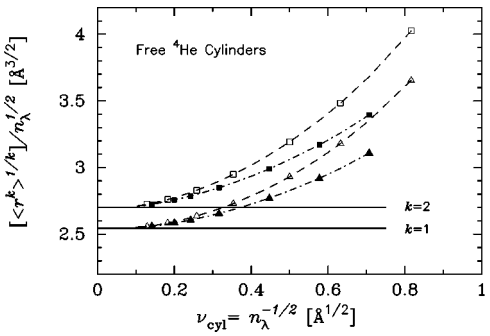

FIG. 1. Normalized moments $[\langle r^k(n_\lambda)\rangle]^{1/k}/n_\lambda^{1/2}$ as a function of the inverse of the square root of longitudinal density $\nu_{\rm cyl}=n_\lambda^{-1/2}$ for free helium cylinders. Open and full symbols stand for Skyrme-DF and OP-NLDF results, respectively. The dashed and dot-dashed curves are only given to guide the eye. The solid lines correspond to the asymptotic values given by Eq. (3.5).

is determined by matching the result of this integral with the k moment of the true radial distribution of the system

$$\langle r^k(N)\rangle_D=\frac{2^{D-1}\pi L^{3-D}}{N}\int_0^\infty dr r^{k+D-1}\rho(r). \qquad (3.2)$$

This condition leads to the generalized Ford-Wills moments [see Eq. (1) in Ref. 29]

$$R_k=\left[\frac{k+D}{D}\langle r^k(N)\rangle_D\right]^{1/k}. \qquad (3.3)$$

A. Cylindrical systems

One expects that very thick cylinders would tend to exhibit features of bulk liquid at saturation conditions. In the asymptotic limit of very large cylinders one expects that Eq. (2.15) will reduce to

$$N/L=2\pi\int_0^{R_0} r dr\rho_0=\pi R_0^2\rho_0, \qquad (3.4)$$

where ρ_0 is the saturation density of bulk ^{4}He quoted in Table I and R_0 is the radius of the uniformly filled cylinder. Since in the limit of very large cylinders the equivalent radius R_k tends toward R_0 defined by Eq. (3.4), one gets the following asymptotic law:

$$\lim_{n_\lambda\to\infty}\left\{\frac{[\langle r^k(n_\lambda)\rangle]^{1/k}}{n_\lambda^{1/2}}\right\}=\sqrt{\frac{1}{\pi\rho_0}}\left(\frac{2}{k+2}\right)^{1/k}. \qquad (3.5)$$

Figure 1 shows how the normalized moments $\langle r\rangle$ and $\langle r^2\rangle$ attain their asymptotic values as a function of the expansion parameter $\nu_{\rm cyl}=n_\lambda^{-1/2}$. One may conclude that the results given by Eq. (3.5) are safely reached for $n_\lambda\simeq 70$ Å^{-1}.

B. Spherical systems

From a similar analysis to that performed for cylinders, one can state that for very large spheres Eq. (2.16) will become

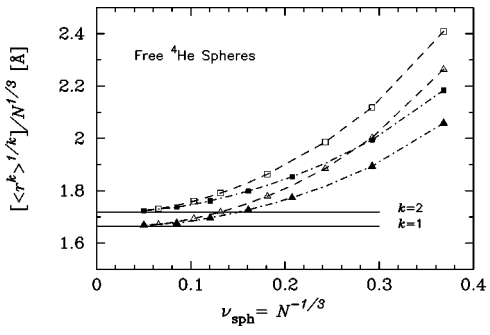

FIG. 2. Similar to Fig. 1, but for free helium spheres. The solid lines correspond to the asymptotic values given by Eq. (3.7).

$$N=4\pi\int_0^{R_0} r^2 dr\rho_0=\frac{4\pi}{3}R_0^3\rho_0, \qquad (3.6)$$

where R_0 is now the radius of the uniformly filled sphere. Furthermore, since in this asymptotic limit R_k tends toward R_0 defined by Eq. (3.6), the following law is obtained:

$$\lim_{N\to\infty}\left\{\frac{[\langle r^k(N)\rangle]^{1/k}}{N^{1/3}}\right\}=\left(\frac{3}{4\pi\rho_0}\right)^{1/3}\left(\frac{3}{k+3}\right)^{1/k}. \qquad (3.7)$$

Figure 2 shows how the normalized moments $\langle r\rangle$ and $\langle r^2\rangle$ attain their asymptotic values as a function of $\nu_{\rm sph}=N^{-1/3}$. The results given by Eq. (3.7) are reached at $N\simeq 2000$. In summary, from values of the normalized moments displayed in Figs. 1 and 2 it is clear that the largest systems examined in the present work have, in practice, reached the asymptotic global behavior.

IV. ANALYSIS OF RESULTS

A. Surface tension

The evolution of the central density, ρ_c, for cylinders with increasing n_λ was explored in Ref. 18. It was found that after a certain value of n_λ the central density becomes larger than the saturation density of infinite helium matter, $\rho_c>\rho_0$, giving rise to a squeezing effect. This phenomenon has been previously found in calculations carried out for atomic nuclei [see Figs. 1(a) and 1(b) in Ref. 30] as well as for spherical clusters of ^{4}He (see Fig. 3 in Ref. 13) and it is known as the ''leptodermous'' behavior. It was demonstrated[18] that for cylinders the squeezing effect, i.e., the difference $\rho_c-\rho_0$, vanishes for $n_\lambda\to\infty$ according to the law

$$\epsilon_{\rm cyl}=\frac{\rho_c-\rho_0}{\rho_0}=\frac{\sigma_\infty}{\mathcal{K}}\sqrt{\frac{\pi}{\rho_0}}n_\lambda^{-1/2}, \qquad (4.1)$$

which is similar to

$$\epsilon_{\rm sph}=\frac{\rho_c-\rho_0}{\rho_0}=2\frac{\sigma_\infty}{\mathcal{K}}\left(\frac{4\pi}{3\rho_0^2}\right)^{1/3}N^{-1/3}, \qquad (4.2)$$

corresponding to ^{4}He spheres [see the asymptotic limit of Eq. (12) in Ref. 13].

In the present work we describe the evolution of the surface tension when the size of the ^{4}He systems is increased. From thermodynamic considerations one sees that

$$dE_{\rm gs} = -PdV + \sigma_A dA + \mu dN, \tag{4.3}$$

where V is the volume of the system, A the surface area enclosing V, and σ_A the surface tension. For both curved geometries the grand free energy takes the form

$$\Omega = E_{\rm gs} - \mu N = -PV + \sigma_A A, \tag{4.4}$$

while $P=0$ for planar slabs. In the following we examine the different cases.

1. Cylindrical systems

In Ref. 18 it was shown that for cylinders the relationship between the grand free energy per unit length and the surface tension becomes

$$\frac{\Omega}{L} = \frac{E_{\rm gs} - \mu N}{L} = (e-\mu) n_\lambda = \pi R_s \sigma_A . \tag{4.5}$$

Here R_s is the sharp mean radius defined by

$$N/L = 2\pi \int_0^{R_s} r dr \rho_c = \pi R_s^2 \rho_c , \tag{4.6}$$

and it is related to R_0 by

$$R_s = R_0 \sqrt{\frac{1}{1+\epsilon_{\rm cyl}}}. \tag{4.7}$$

Furthermore, it was demonstrated in Ref. 18 that for large cylindrical systems (in the sense of large R_s) the total energy per particle may be expressed as

$$e = \frac{E_{\rm gs}}{N} = e_B + 2\sigma_\infty \sqrt{\frac{\pi}{\rho_0}} n_\lambda^{-1/2} + \left(\varepsilon_\ell - \frac{\pi \sigma_\infty^2}{2\rho_0 \mathcal{K}} \right) n_\lambda^{-1} + \cdots , \tag{4.8}$$

where σ_∞ and ε_ℓ are, respectively, the asymptotic surface tension and the residual energy per unit length defined in Ref. 18. A formula for the surface tension σ_A may be derived by taking into account Eq. (5.7) of Ref. 18,

$$\pi R_s \sigma_A = -n_\lambda^2 \frac{de}{dn_\lambda}, \tag{4.9}$$

and the present relationship (4.5). After keeping all terms up to second order in $\nu_{\rm cyl} = n_\lambda^{-1/2}$ one gets

$$\begin{aligned} \sigma_A &= \frac{2\Omega}{A_{\rm cyl}} = \frac{2(e-\mu)N}{2\pi R_s L} = -\frac{n_\lambda^2}{\pi R_s} \frac{de}{dn_\lambda} \\ &= \sigma_\infty + \sqrt{\frac{\rho_0}{\pi}} \varepsilon_\ell n_\lambda^{-1/2} + \frac{\sigma_\infty}{2\mathcal{K}} \left(\varepsilon_\ell - \frac{3}{4} \frac{\pi \sigma_\infty^2}{\rho_0 \mathcal{K}} \right) n_\lambda^{-1} . \end{aligned} \tag{4.10}$$

This expression indicates that the asymptotic result $\sigma_A(n_\lambda \to \infty) = \sigma_\infty$, which may be identified with the experimental[8–10] values of the surface tension $\sigma_{\rm exp}$ quoted in Table I, should be attained linearly in the parameter $\nu_{\rm cyl} = n_\lambda^{-1/2}$ with a slope proportional to ε_ℓ,

$$\sigma_A \simeq \sigma_\infty + \sqrt{\frac{\rho_0}{\pi}} \varepsilon_\ell n_\lambda^{-1/2}. \tag{4.11}$$

The values of ε_ℓ obtained from the fits of energies per particle to Eq. (4.8) are listed in Table I. Since these results are positive one expects an overshoot [i.e., a region in which $\sigma_A(n_\lambda) > \sigma_\infty$] for large cylinders.

2. Spherical systems

In the case of spherical systems, upon starting from Eqs. (4.3) and (4.4) one arrives at

$$d\Omega = d(E_{\rm gs} - \mu N) = -PdV + \sigma_A dA - N d\mu . \tag{4.12}$$

At equilibrium, for fixed μ, the virtual work resulted from changing the radius of the sphere should vanish,

$$-PdV + \sigma_A dA = -P 4\pi R_s^2 dR_s + \sigma_A 8\pi R_s dR_s = 0. \tag{4.13}$$

This equation leads to

$$P = \frac{2\sigma_A}{R_s}, \tag{4.14}$$

where the sharp mean radius is

$$R_s = R_0 \left(\frac{1}{1+\epsilon_{\rm sph}} \right)^{1/3}, \tag{4.15}$$

with R_0 defined by Eq. (3.6). Then by using Eq. (4.4) one gets

$$\begin{aligned} \Omega = -PV + \sigma_A A &= -\left(\frac{2\sigma_A}{R_s} \right) \left(\frac{4\pi}{3} \right) R_s^3 + \sigma_A 4\pi R_s^2 \\ &= \frac{4\pi}{3} R_s^2 \sigma_A . \end{aligned} \tag{4.16}$$

The total energy per particle can be expanded in the following way [cf. Eq. (13) of Ref. 13]:

$$\begin{aligned} e = \frac{E_{\rm gs}}{N} &= e_B + \sigma_\infty \left(\frac{36\pi}{\rho_0^2} \right)^{1/3} N^{-1/3} \\ &+ \left[a_c - 2\frac{\sigma_\infty^2}{\mathcal{K}} \left(\frac{4\pi}{3\rho_0^2} \right)^{2/3} \right] N^{-2/3} + \cdots . \end{aligned} \tag{4.17}$$

Hence, for spherical systems one gets

$$\begin{aligned} \sigma_A &= \frac{3\Omega}{A_{\rm sph}} = \frac{3(e-\mu)N}{4\pi R_s^2} \\ &= -\frac{3N^2}{4\pi R_s^2} \frac{de}{dN} \simeq \sigma_\infty + a_c \left(\frac{2\rho_0^2}{9\pi} \right)^{1/3} N^{-1/3}. \end{aligned} \tag{4.18}$$

The values of a_c determined by fitting energies per particle of drops with $N \geqslant 300$ to Eq. (4.17) are quoted in Table I.

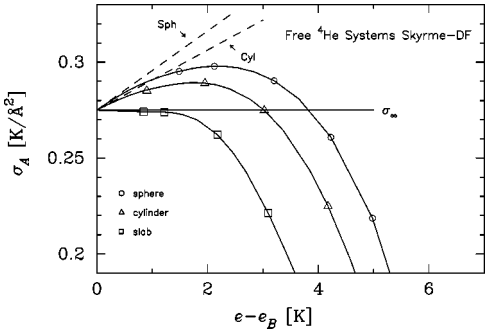

FIG. 3. Surface tension calculated using the Skyrme DF is shown as a function of the energy difference $e-e_B$. In order to avoid overcrowding the picture only some selected data are plotted and solid curves are drawn to guide the eye. Dashed lines indicate the linear asymptotic laws for curved geometries given by Eqs. (4.21) and (4.22).

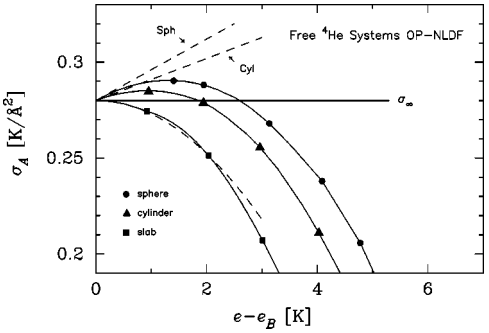

FIG. 4. Same as Fig. 3 with data calculated using the OP NLDF. In addition, the dashed curve for planar slabs is the quadratic asymptotic law given by Eq. (4.23).

Since these results are positive, overshoots of σ_A should be expected. For the sake of comparison prior results reported in Refs. 13 and 21 obtained by using the Skyrme DF and considering systems with $N \leqslant 728$ are also included in Table I. All these data are in good agreement.

3. Comparison of results for regular geometries

Let us now summarize the results for the surface tension for the three regular geometries. Instead of showing the surface tension separately for each geometry as a function of the appropriate expansion parameter ν, we find it more interesting to present all the data in a unified picture. In order to achieve this goal it is useful to consider that for all three symmetries (planar, cylindrical, and spherical) the final trend of the energy per particle toward the asymptotic value, i.e., the bulk e_B, is mainly determined by the linear term in the corresponding expansion parameter. Therefore, it becomes reasonable to adopt the energy difference $e-e_B$ as an appropriate common abscissa. In order to facilitate the forthcoming discussion we recall that for a symmetric planar slab (see, e.g., Ref. 5) the energy per particle may be expressed as an expansion in terms of inverse coverage $n_c^{-1}=A_{\rm slab}/N$,

$$e=\frac{E_{\rm gs}}{N}=e_B+2\sigma_\infty n_c^{-1}+\gamma_c n_c^{-3}+\cdots, \tag{4.19}$$

and the total surface tension becomes

$$\sigma_A^{(\rm tot)}=\frac{\Omega}{A_{\rm slab}}=\frac{E_{\rm gs}-\mu N}{A_{\rm slab}}=\frac{(e-\mu)N}{L^2}=-n_c^2\frac{de}{dn_c}\simeq 2\sigma_\infty + 3\gamma_c n_c^{-2}. \tag{4.20}$$

Values for the surface tension obtained from calculations carried out using the Skyrme DF are displayed in Fig. 3, while Fig. 4 shows the behavior of σ_A evaluated using the finite range OP NLDF. The main features exhibited by both these drawings are similar. In particular, for curved geometries the surface tension tends toward σ_∞ showing the predicted overshoot, which is similar to that previously found for ρ_c (see Fig. 6 in Ref. 18 and Fig. 3 in Ref. 13). Furthermore, in both figures the final trends toward σ_∞ match the linear asymptotic expressions

(i) for cylindrical systems

$$\sigma_A\simeq\sigma_\infty+\frac{\rho_0\varepsilon_\ell}{2\pi\sigma_\infty}(e-e_B), \tag{4.21}$$

(ii) and for spherical systems

$$\sigma_A\simeq\sigma_\infty+\frac{\rho_0 a_c}{3\pi\sigma_\infty}\left(\frac{\pi\rho_0}{6}\right)^{1/3}(e-e_B). \tag{4.22}$$

On the other hand, the data for planar slabs attain the asymptotic value in a smooth way with zero slope, that is, without any linear term. This behavior may be understood on the basis of the fact that upon starting from Eq. (4.20) one gets

(iii) for planar systems

$$\sigma_A=\frac{\sigma_A^{(\rm tot)}}{2}\simeq\sigma_\infty+\frac{3\gamma_c}{8\sigma_\infty^2}(e-e_B)^2. \tag{4.23}$$

Here σ_A is the surface tension at each free interface. The values obtained with the OP-NLDF approach match this law with $\gamma_c=-1.44\times10^{-3}$ K/Å^6 listed in Table 2 of Ref. 5, while the trend of results provided by the Skyrme DF is even flatter suggesting a $(e-e_B)^n$ law with $n\geqslant 3$. The latter behavior results from the fact that in such a mean-field approximation $\gamma_c\simeq 0$ because the Lennard-Jones potential is not included in the theory (cf. Table 2 and the discussion in Ref. 5).

4. Relation between a_c and ε_ℓ

We now search for a relation between a_c and ε_ℓ. According to the droplet model[30,31] (DM) the total ground-state energy of a large system may be written as a sum of volume, surface, and curvature terms,

$$E_{\rm gs}=E_v+E_s+E_c. \tag{4.24}$$

The surface and curvature energies for cylindrical systems may be written as [see Eq. (4.8) in Ref. 18]

$$E_s(\mathrm{cyl}) = 2\pi R_0 L \int_0^\infty \{\rho(r)\mathcal{H}[\rho,\boldsymbol{\nabla}\rho] - \rho_0 e_0\} dr$$

$$= 2\pi R_0(\mathrm{cyl}) L \sigma_\infty , \tag{4.25}$$

$$E_c(\mathrm{cyl}) = 2\pi L \int_0^\infty \{\rho(r)\mathcal{H}[\rho,\boldsymbol{\nabla}\rho] - \rho_0 e_0\}(r - R_0) dr = \varepsilon_\ell L, \tag{4.26}$$

while for spheres Eq. (2.11) in Ref. 31 holds that

$$E_s(\mathrm{sph}) = 4\pi R_0^2 \int_0^\infty \{\rho(r)\mathcal{H}[\rho,\boldsymbol{\nabla}\rho] - \rho_0 e_0\} dr$$

$$= 4\pi R_0^2(\mathrm{sph})\sigma_\infty = a_s N^{2/3}, \tag{4.27}$$

$$E_c(\mathrm{sph}) = 8\pi R_0 \int_0^\infty \{\rho(r)\mathcal{H}[\rho,\boldsymbol{\nabla}\rho] - \rho_0 e_0\}(r - R_0) dr$$

$$= a_c N^{1/3}. \tag{4.28}$$

In this approach the integrals in Eqs. (4.25) and (4.27) are associated with σ_∞, and it was verified numerically that they yield equal results. The integrals in Eqs. (4.26) and (4.28) may be considered to be higher-order moment of the former integrals, hence, it becomes plausible to suppose that they should exhibit similar features. Therefore, one would be able to write

$$E_c(\mathrm{cyl}) = \pi L \lambda_\infty = \varepsilon_\ell L, \tag{4.29}$$

and

$$E_c(\mathrm{sph}) = 4\pi R_0(\mathrm{sph})\lambda_\infty = a_c N^{1/3}. \tag{4.30}$$

Here λ_∞ is twice the asymptotic value of the integrals in Eqs. (4.26) and (4.28) and may be interpreted as the asymptotic coefficient for the curvature energy. It is worth noticing that the curvature energy may be expressed in terms of the area and curvature of the cylindrical and spherical surfaces. According to a theorem of Euler the average curvature at a given point of a surface is defined as[32]

$$\mathcal{C} = \frac{1}{2}\left(\frac{1}{R_1} + \frac{1}{R_2}\right), \tag{4.31}$$

where R_1 and R_2 are the radii of curvature along any two orthogonal tangents. Hence, for wide cylinders one gets

$$\mathcal{C}_{\mathrm{cyl}} = \frac{1}{2}\left(\frac{1}{R_\varphi} + \frac{1}{R_{z\to\infty}}\right) = \frac{1}{2R_0(\mathrm{cyl})}; \tag{4.32}$$

for large spheres

$$\mathcal{C}_{\mathrm{sph}} = \frac{1}{2}\left(\frac{1}{R_\varphi} + \frac{1}{R_\theta}\right) = \frac{1}{R_0(\mathrm{sph})}, \tag{4.33}$$

while for planar slabs it holds that $\mathcal{C}_{\mathrm{slab}} = 0$. So, one may write

$$E_c(\mathrm{cyl}) = 2\pi R_0(\mathrm{cyl}) L \frac{1}{2R_0(\mathrm{cyl})}\lambda_\infty = A_{\mathrm{cyl}}\mathcal{C}_{\mathrm{cyl}}\lambda_\infty , \tag{4.34}$$

and

$$E_c(\mathrm{sph}) = 4\pi R_0^2(\mathrm{sph})\frac{1}{R_0(\mathrm{sph})}\lambda_\infty = A_{\mathrm{sph}}\mathcal{C}_{\mathrm{sph}}\lambda_\infty . \tag{4.35}$$

The relation between a_c and ε_ℓ may be derived from the ratio of this equation:

$$\frac{E_c(\mathrm{sph})}{E_c(\mathrm{cyl})} = \frac{A_{\mathrm{sph}}\mathcal{C}_{\mathrm{sph}}\lambda_\infty}{A_{\mathrm{cyl}}\mathcal{C}_{\mathrm{cyl}}\lambda_\infty} = \frac{4R_0(\mathrm{sph})}{L} = \frac{a_c N^{1/3}}{\varepsilon_\ell L}, \tag{4.36}$$

which yields

$$\frac{a_c}{\varepsilon_\ell} = \frac{4R_0(\mathrm{sph})}{N^{1/3}} = 4\left(\frac{3}{4\pi\rho_0}\right)^{1/3}, \tag{4.37}$$

leading to

$$\left(\frac{\pi\rho_0}{48}\right)^{1/3}\frac{a_c}{\varepsilon_\ell} = 1. \tag{4.38}$$

The values of this relation calculated with parameters determined from both examined DFs are included in Table I. For the Skyrme DF the result was 0.99, in excellent agreement with the DM prediction. The ratio yielded by the OP NLDF, i.e., 1.10, differs slightly from unity. This is indeed to be expected when the DF is not only written in terms of $\rho(r)$ but has explicit information on r as happens with the Lennard-Jones potential. In such a case there is an additional curvature contribution which in the approach adopted here is embedded in the coefficient a_c.[31]

Upon starting from Eqs. (4.11) and (4.18), in both cases, one may express the excess of surface energy in terms of the curvature and the quantity λ_∞, and get

$$(\sigma_A - \sigma_\infty)_{\mathrm{cyl}} \simeq \sqrt{\frac{\rho_0}{\pi}}\varepsilon_\ell n_\lambda^{-1/2} = \frac{\varepsilon_\ell}{\pi R_0(\mathrm{cyl})} = \frac{2\varepsilon_\ell}{\pi}\mathcal{C}_{\mathrm{cyl}}$$

$$= 2\lambda_\infty \mathcal{C}_{\mathrm{cyl}}, \tag{4.39}$$

$$(\sigma_A - \sigma_\infty)_{\mathrm{sph}} \simeq a_c\left(\frac{2\rho_0^2}{9\pi}\right)^{1/3} N^{-1/3}$$

$$= \left(\frac{\pi\rho_0}{6}\right)^{1/3}\frac{a_c}{\pi R_0(\mathrm{sph})} = \left(\frac{\pi\rho_0}{6}\right)^{1/3}\frac{a_c}{\pi}\mathcal{C}_{\mathrm{sph}}$$

$$= 2\lambda_\infty \mathcal{C}_{\mathrm{sph}}. \tag{4.40}$$

By taking into account these results one arrives at

$$\frac{(\sigma_A - \sigma_\infty)_{\mathrm{sph}} A_{\mathrm{sph}}}{(\sigma_A - \sigma_\infty)_{\mathrm{cyl}} A_{\mathrm{cyl}}} = \frac{A_{\mathrm{sph}}\mathcal{C}_{\mathrm{sph}}}{A_{\mathrm{cyl}}\mathcal{C}_{\mathrm{cyl}}} = \frac{E_c(\mathrm{sph})}{E_c(\mathrm{cyl})}. \tag{4.41}$$

This means that the ratio of the excess of surface energies is equal to the ratio of curvature energies.

B. Thickness at the free interface

All the calculated results for the surface thickness W of free ^{4}He systems are plotted together in Fig. 5 as a function of $e - e_B$. Let us first look at values obtained by applying the

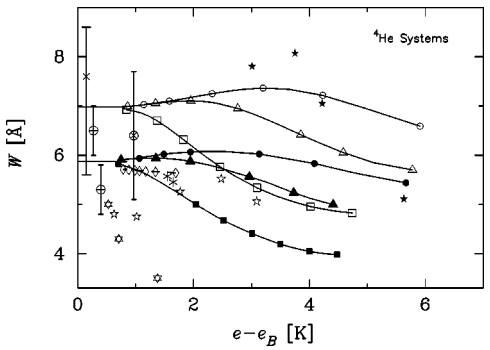

FIG. 5. Thickness of the free surface as a function of the energy difference $e-e_B$. The circles, triangles, and squares represent our own data for spherical, cylindrical, and planar systems, respectively. Empty symbols stand for data calculated using the Skyrme DF, while full symbols are results from the OP-NLDF approach. As in previous figures, only some selected data are plotted and solid curves are drawn to guide the eye. Diamonds are OT-NLDF results for spheres from Ref. 4. Full and empty five-point stars are Monte Carlo simulations for spheres and slabs reported in Ref. 6. Six-points star are Monte Carlo data from Ref. 12. Asterisks are OP-NLDF results for helium adsorbed onto planar Na and Li substrates. $(\times)$, $(\otimes)$, and $(\oplus)$ are experimental values from Refs. 3, 4, and 7, respectively.

Skyrme DF. In this case we must state a word of caution because our results for spheres differ noticeably from those listed in the fifth column of Table I in Ref. 13. We attribute this difference to a misprint in Table I of Ref. 13 in view of the fact that the tabulated values are also inconsistent with the thickness inferred from the profiles plotted in Fig. 1 of the same paper. This point is stressed because due to that mistake the range of W ascribed to calculations with the Skyrme-DF for spheres with $N \leqslant 728$ quoted in the summary of Table III in Ref. 4 is incorrect, actually it is $6.6 \lesssim W \lesssim 7.4$ Å.

Turning to the present results, the displayed data indicate that the asymptotic surface width obtained with the zero-range functional does not depend on the geometry of the helium system. In all the cases it attains $W_\infty \simeq 7$ Å, in agreement with the asymptotic result for an infinite system reported in Ref. 13.

The results obtained from calculations carried out with the OP NLDF are smaller than those yielded by the Skyrme DF, but exhibit a similar trend as a function of $e-e_B$ and the asymptotic width is also independent of the geometry, being $W_\infty \simeq 5.9$ Å. For large systems the OP-NLDF thickness is close to that reported for droplets in Table II of Harms *et al.*[4] These authors have performed calculations for large systems ($1000 \leqslant N \leqslant 10\,000$, i.e., $-6.4 \lesssim e \lesssim -5.4$ K) with the more elaborate OT NLDF, getting $W \simeq 5.7$ Å, as may be seen in the drawing.

The values obtained from Monte Carlo simulations for free planar slabs[6,12] and spherical drops[6] are also plotted in Fig. 5. However, in particular, the data evaluated by using glue-SWF (Ref. 6) exhibit a spread too large to facilitate meaningful systematics.

A comparison between the theoretical results mentioned above and the experimental data is performed in Fig. 5. The data obtained in the measurement of large droplets published in Ref. 4 are represented by the reported mean thickness $W = 6.4 \pm 1.3$ Å. In the case of Ref. 7 only the two data included by the authors in the abstract are shown. Since these values correspond to rather broad planar films, we plotted them schematically close to the origin for the abscissa. A similar criterion was adopted for the value of Ref. 3. As can be seen in this figure, all the results provided by finite range functionals for the largest systems are consistent with the most recent and precise experimental data.[7]

The measurements of Refs. 3 and 7 have been performed for planar films of ^{4}He adsorbed onto a substrate of Si, while the calculations mentioned above have been carried out for free planar slabs. Therefore we completed the investigation exploring the extent that theoretical results change when helium is adsorbed on a solid surface. In doing so, we include in this analysis the results of our OP-NLDF estimations of the thickness at the free interface for ^{4}He films adsorbed on surfaces of Na and Li. These substrates provide the strongest adsorption potentials among alkali metals.[33,34] For example, we show in Fig. 5 the values calculated for stable films with coverage $n_c = 0.34$ Å^{-2} in the case of both substrates, i.e., $W = 5.57$ (Na) and 5.45 Å (Li).[35] These results fit perfectly into the general pattern exhibited by evaluations performed with NLDF and recent experimental data.[7]

1. Simple models for the surface thickness

Let us now show that very simple models provide reasonable estimations of the interface thickness and its relation with the surface tension for large systems. For this purpose, it is useful to start first from Eq. (2.6) of Ref. 5 for σ_A of planar slabs obtained within the Skyrme DF. It reads

$$\sigma_A = \frac{1}{2}\int_{-\infty}^{\infty} dz \left\{ \frac{\hbar^2}{m}\left[\frac{d\sqrt{\rho(z)}}{dz}\right]^2 + 2d_4\left[\frac{d\rho(z)}{dz}\right]^2 \right\}. \tag{4.42}$$

We evaluate this integral adopting a crude approximation for the density profile of a wide slab. Let us consider that from $z=0$ to $z=z_0$ the density is constant and equal to its value at the center, ρ_c. Subsequently, for $z>z_0$ the falloff begins. Assuming that the first stretch of the falloff up to $z=z_\ell$ is linear, provided that $\rho(z_\ell) < \rho_c/10$, one may write

$$\rho(z) = \rho_c\left(1 - \frac{z-z_0}{\tilde{W}}\right) = \rho_c\left[1 - \frac{4(z-z_0)}{5W}\right]. \tag{4.43}$$

Next, for $z \geqslant z_\ell$, the falloff of the density profile follows the asymptotic exponential law [see, for instance, Eqs. (7) and (9) of Ref. 36]

$$\rho(z) = \frac{\rho_c}{\alpha}\exp[-2B(z-z_\ell)], \tag{4.44}$$

with $B = \sqrt{-2me_B/\hbar^2} = 1.09$ Å^{-1}. The parameters z_ℓ and α are determined by matching at $z=z_\ell$ the expressions (4.43) and (4.44) for $\rho(z)$ as well as its derivatives $d\rho(z)/dz$. This task is performed in Appendix B and the result is

$$\sigma_A \simeq \frac{\rho_c}{5W}\left(\frac{\hbar^2}{m}+8d_4\rho_c\right). \tag{4.45}$$

So, in this crude approach the asymptotic width becomes

$$W_\infty \simeq \frac{\rho_0}{5\sigma_\infty}\left(\frac{\hbar^2}{m}+8d_4\rho_0\right)=6.83 \text{ Å}, \tag{4.46}$$

lying close to the limit suggested by data displayed in Fig. 5.

A slightly different version of the simple model described above may provide separate formulas for the surface thickness and tension in terms of parameters of the Skyrme DF. As we see below, such expressions are valid for all the analyzed geometries. In this model, the proposed $\rho(r)$ is the simplest that takes into account three of the most relevant characteristics of the density profile: the sharp radius of the density distribution R_s, the thickness of the interface W, and the "leptodermous" behavior $\rho_c > \rho_0$. We assume that from $r=0$ to $r=R_1=R_s-\beta\tilde{W}$ the density is constant and equal to $\rho_c=\rho(r=0)$, and we recall that $\tilde{W}=5W/4$. At $r=R_1$ a linear falloff begins and for $r \geqslant R_2=R_s+(1-\beta)\tilde{W}$ the density vanishes. The parameter β depends on the geometry through the normalization condition given by Eq. (2.3), where N should be suitably written for nonspherical systems in terms of n_c or n_λ. The obtained formulas for the normalization condition and the parameter β are given in Appendix C. Subsequently, the ground-state energy provided by the Skyrme DF for slabs, cylinders, and spheres was expressed by taking into account the proposed $\rho(r)$. In order to avoid an unphysical divergence in the integration of the kinetic term caused by the kink of the adopted density profile we assumed that

$$\frac{d\sqrt{\rho(z)}}{dz} \simeq -\frac{4\sqrt{\rho(z)}}{5W}. \tag{4.47}$$

As an example, the energy for cylinders is given in Appendix C.

Upon minimizing the grand free energy [e.g., for cylinders, see Eq. (C5)] with respect to W and ϵ, and keeping only the dominant terms, the following relation valid for all three considered geometries is obtained:

$$W\sigma_A=\frac{4\rho_c}{5}\left(\frac{\hbar^2}{m}+2d_4\rho_c\right). \tag{4.48}$$

Here, the dominant contribution which is given by the term proportional to d_4 is equal to that previously obtained in Eq. (4.45). This procedure also yields an expression for the asymptotic width in terms of parameters of the functional,

$$W_\infty=\frac{4}{5}\frac{\sqrt{(\hbar^2/m)+2d_4\rho_0}}{\sqrt{-e_B+\frac{b_4}{3}\rho_0+\frac{c_4}{\gamma_4+3}\rho_0^{\gamma_4+1}}}=6.90 \text{ Å}. \tag{4.49}$$

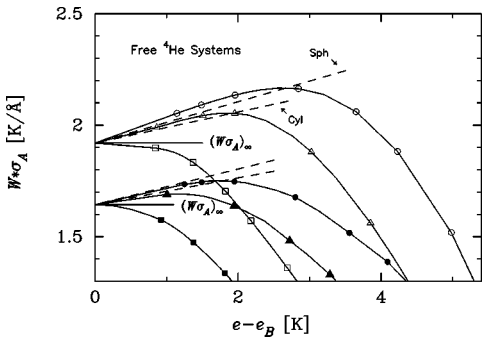

FIG. 6. Quantity $W\sigma_A$ as a function of the energy difference $e-e_B$. As in Fig. 5, the circles, triangles, and squares represent data for spherical, cylindrical, and planar systems, respectively. Empty symbols stand for data calculated using the Skyrme DF, while full symbols are results from the OP-NLDF approach. Dashed lines indicate the linear asymptotic laws for curved geometries given by Eqs. (4.53) and (4.54).

This value is in excellent agreement with the asymptotic result obtained from the complete numerical solutions in the Skyrme-DF approach. The corresponding result for the asymptotic surface tension,

$$\sigma_\infty=\frac{4}{5}\frac{\rho_0}{W_\infty}\left(\frac{\hbar^2}{m}+2d_4\rho_0\right)=0.294 \text{ K/Å}^2, \tag{4.50}$$

indicates a good degree of self-consistency of this approximation. In conclusion, we can state that the crude simple models used here to estimate the surface thickness are able to account for a substantial part of the physics involved.

2. The quantity $W\sigma_A$

By looking at the relation between W and σ_A given by Eqs. (4.45) and (4.48), we found it worthy to examine the product $W\sigma_A$ as a function of $e-e_B$. Such a behavior is shown in Fig. 6, where for curved geometries one may observe overshoots similar to that exhibited by the central density and the surface tension. Since according to Eqs. (4.45) and (4.48) the main contribution to $W\sigma_A$ is given by the term containing d_4, in this case the linear departure would be governed by

$$\rho_c^2=\rho_0^2(1+\epsilon)^2 \simeq \rho_0^2(1+2\epsilon), \tag{4.51}$$

which leads to

$$W\sigma_A \simeq (W\sigma_A)_\infty(1+2\epsilon). \tag{4.52}$$

This relation yields linear asymptotic expressions, where the slope is determined by the compressibility $\mathcal{K}$ which is an input for the adopted DF approaches

(i) for cylindrical systems

$$W\sigma_A \simeq (W\sigma)_\infty\left[1+\frac{1}{\mathcal{K}}(e-e_B)\right]; \tag{4.53}$$

(ii) and for spherical systems

$$W\sigma_A \simeq (W\sigma)_\infty \left[1 + \frac{4}{3\mathcal{K}}(e - e_B) \right]. \tag{4.54}$$

These approximations are plotted as dashed lines in Fig. 6. From this drawing one can realize that these very simple forms account fairly well for the obtained departures. In the case of planar systems there is no overshoot.

By combining the expansions for the product $W\sigma_A$ and for the surface tension σ_A it is possible to estimate the departure of W from its asymptotic value

(i) for cylindrical systems

$$W = \frac{(W\sigma_A)}{\sigma_A} \simeq W_\infty \left[1 + \left(\frac{1}{\mathcal{K}} - \frac{\rho_0 \varepsilon_\ell}{2\pi\sigma_\infty^2} \right)(e - e_B) \right]; \tag{4.55}$$

(ii) and for spherical systems

$$W = \frac{(W\sigma_A)}{\sigma_A} \simeq W_\infty \left\{ 1 + \left[\frac{4}{3\mathcal{K}} - \frac{\rho_0 a_c}{3\pi\sigma_\infty^2} \left(\frac{\pi\rho_0}{6} \right)^{1/3} \right](e - e_B) \right\}. \tag{4.56}$$

For both geometries there is an important cancellation within the coefficient of the linear term in these expressions. This fact explains why for large systems the thickness as a function of $e - e_B$ is flat in Fig. 5.

V. SUMMARY

The curvature effects on the thickness of the free interface W and the corresponding surface tension σ_A are studied. It is known that the free spherical systems are those with the lowest surface area to volume ratio which leads to the lowest energy per particle, but nevertheless, we found it interesting to also examine other geometries to get a more complete view of surface properties. In addition, some general properties of free systems could be extended to adsorbed ones.

First of all, we tested whether the largest systems have already reached the critical size for exhibiting a global asymptotic behavior. From Figs. 1 and 2 one may realize that the moments $\langle r^k \rangle$, with $k = 1$ and 2, have attained the asymptotic values.

In this paper, the results for σ_A and W corresponding to different geometries are presented in a unified scale as a function of $e - e_B$ allowing a direct comparison. As far as we know, this procedure has not been previously used.

It was found that for cylindrical and spherical systems the surface tension presents an overshoot similar to that previously observed for the central density.[13,18] This fact indicates that the squeezing effect known as ''leptodermous'' behavior is also manifested in the surface tension. On the contrary, this feature is not present in the case of symmetric planar slabs. It is shown that the behavior of large systems may be well interpreted within the DM,[30,31] adapted to each geometry. In particular, a relation between coefficients of the curvature energy is derived.

An analysis of the surface thickness W indicates that for large systems, i.e., when $e - e_B \lesssim 1$ K, the asymptotic result is independent of the geometry of the ^{4}He system. The departure from that value is different for each geometry. These features are common to both examined density functionals. We should mention that according to a discussion given in the text, the range $8.8 \lesssim W \lesssim 9.2$ Å quoted in Table III of Ref. 4 as corresponding to droplets (with $N \leqslant 728$) studied by utilizing the Skyrme DF, which was determined with data taken from Table I of Ref. 13, must be replaced by $6.6 \lesssim W \lesssim 7.4$ Å.

The results obtained with the OP NLDF for large systems are close to those calculated with the OT NLDF for spheres by Harms *et al.*[4] It is shown in Fig. 5 that the most recent experimental data[7] favor the results yielded by the finite range density functionals. In addition, the thickness of the free surface of helium films adsorbed on planar substrates of Na and Li evaluated with the OP NLDF matches very well with the pattern depicted in Fig. 5.

We have also analyzed the product $W\sigma_A$. As expected, for curved geometries this quantity exhibits an overshoot. However, it is interesting to note that in this case the departure from the asymptotic values is mainly determined by the inverse of the compressibility $\mathcal{K}$ of bulk ^{4}He. Furthermore, this analysis gives a hint for understanding the flat behavior of W at small $e - e_B$.

ACKNOWLEDGMENT

This work was supported in part by the Ministry of Culture and Education of Argentina through Grant Nos. PICT-2000-03-08450 from ANPCYT and X103 from the University of Buenos Aires.

APPENDIX A: OP-NLDF HARTREE MEAN-FIELD POTENTIAL

In this Appendix we compile the relevant expressions derived in the OP-NLDF approach for a spherical geometry. The explicit form of the Hartree mean-field potential $V_H(r)$ derived according to Eq. (2.5) becomes

$$V_H^{\mathrm{OP}}(r) = \frac{\delta E_{sc}[\rho]}{\delta\rho(r)} = \int d\mathbf{r}'\, \rho(r')\, V_l^{\mathrm{OP}}(|\mathbf{r} - \mathbf{r}'|) + \frac{c_4}{2}[\overline{\rho}(r)]^{\gamma_4 + 1} + \frac{c_4}{2}(\gamma_4 + 1) \int d\mathbf{r}'\, \rho(r') \times [\overline{\rho}(r')]^{\gamma_4} \mathcal{W}(|\mathbf{r} - \mathbf{r}'|). \tag{A1}$$

Let us first provide the expressions of the contributions involving the ''coarse-grained density'' $\overline{\rho}(r)$, i.e.,

$$\overline{\rho}(r) = \int d\mathbf{r}'\, \rho(r')\, \mathcal{W}(|\mathbf{r} - \mathbf{r}'|), \tag{A2}$$

and

$$\overline{\rho}_V(r) = \int d\mathbf{r}'\, \rho(r')[\overline{\rho}(r')]^{\gamma_4} \mathcal{W}(|\mathbf{r} - \mathbf{r}'|). \tag{A3}$$

Both these integrals may be cast into the form

$$\overline{\mathcal{R}}(r)=\frac{3}{4\pi h_{\mathrm{OP}}^3}\int d\mathbf{r}'\mathcal{R}(r')\Theta(h_{\mathrm{OP}}-|\mathbf{r}-\mathbf{r}'|). \quad \text{(A4)}$$

After introducing spherical coordinates and taking into account the fact that the step function is symmetric in the azimuthal angle φ, the integration over this variable yields

$$\overline{\mathcal{R}}(r)=\frac{3}{2h_{\mathrm{OP}}^3}\int_{r'_{\min}}^{r'_{\max}} r'^2 dr'\mathcal{R}(r') \times\int_0^{\theta_{\max}}\sin\theta d\theta\Theta[h_{\mathrm{OP}}^2-r^2-r'^2+2rr'\cos\theta]. \quad \text{(A5)}$$

For the point located at $r=0$ one gets

$$\overline{\mathcal{R}}(r=0)=\frac{3}{2h_{\mathrm{OP}}^3}\int_{r'_{\min}}^{r'_{\max}} r'^2 dr'\mathcal{R}(r')\Theta[h_{\mathrm{OP}}^2-r'^2]\int_0^{\pi}\sin\theta d\theta =\frac{3}{h_{\mathrm{OP}}^3}\int_0^{h_{\mathrm{OP}}} r'^2 dr'\mathcal{R}(r'). \quad \text{(A6)}$$

For $r>0$ two different cases should be considered: (i) $0<r<h_{\mathrm{OP}}$ and (ii) $r\geqslant h_{\mathrm{OP}}$. For $0<r<h_{\mathrm{OP}}$ the integral over r' should be split into two parts,

$$\overline{\mathcal{R}}(r)=\frac{3}{2h_{\mathrm{OP}}^3}\left\{\int_0^{h_{\mathrm{OP}}-r}+\int_{h_{\mathrm{OP}}-r}^{r+h_{\mathrm{OP}}}\right\} r'^2 dr'\mathcal{R}(r') \times\int_0^{\theta_{\max}}\sin\theta d\theta\Theta[h_{\mathrm{OP}}^2-r^2-r'^2+2rr'\cos\theta]. \quad \text{(A7)}$$

Since for the first integral over r' the upper angular limit is $\theta_{\max}=\pi$, while for the second integral $\theta_{\max}$ is determined by the condition

$$\cos\theta_{\max}=\frac{r^2+r'^2-h_{\mathrm{OP}}^2}{2rr'}, \quad \text{(A8)}$$

then

$$\overline{\mathcal{R}}(r)=\frac{3}{2h_{\mathrm{OP}}^3}\int_0^{h_{\mathrm{OP}}-r} r'^2 dr'\mathcal{R}(r')\int_0^{\pi}\sin\theta d\theta + \frac{3}{2h_{\mathrm{OP}}^3}\int_{h_{\mathrm{OP}}-r}^{r+h_{\mathrm{OP}}} r'^2 dr'\mathcal{R}(r')\int_0^{\theta_{\max}}\sin\theta d\theta. \quad \text{(A9)}$$

The integration over θ leads to the very simple expression

$$\overline{\mathcal{R}}(r)=\frac{3}{h_{\mathrm{OP}}^3}\int_0^{h_{\mathrm{OP}}-r} r'^2 dr'\mathcal{R}(r') + \frac{3}{4rh_{\mathrm{OP}}}\int_{h_{\mathrm{OP}}-r}^{r+h_{\mathrm{OP}}} r' dr'\mathcal{R}(r')\left[1-\left(\frac{r-r'}{h_{\mathrm{OP}}}\right)^2\right]. \quad \text{(A10)}$$

For $r\geqslant h_{\mathrm{OP}}$, there is only one contribution similar to the second term in Eq. (A9), that is,

$$\overline{\mathcal{R}}(r)=\frac{3}{2h_{\mathrm{OP}}^3}\int_{r-h_{\mathrm{OP}}}^{r+h_{\mathrm{OP}}} r'^2 dr'\mathcal{R}(r')\int_0^{\theta_{\max}}\sin\theta d\theta =\frac{3}{4rh_{\mathrm{OP}}}\int_{r-h_{\mathrm{OP}}}^{r+h_{\mathrm{OP}}} r' dr'\mathcal{R}(r')\left[1-\left(\frac{r-r'}{h_{\mathrm{OP}}}\right)^2\right]. \quad \text{(A11)}$$

Let us now focus on the integration of the screened LJ potential contributing to Eq. (A1):

$$V_H^{\mathrm{LJ\,Scr}}(r)=\int d\mathbf{r}'\rho(r')V_l^{\mathrm{OP}}(|\mathbf{r}-\mathbf{r}'|) =V_l^{\mathrm{OP}}(h_{\mathrm{OP}})\int d\mathbf{r}'\rho(r')\left(\frac{R}{h_{\mathrm{OP}}}\right)^4\Theta(h_{\mathrm{OP}}-R)+4\epsilon \times\int_{R\geqslant h_{\mathrm{OP}}} d\mathbf{r}'\rho(r')\left[\left(\frac{\sigma}{R}\right)^{12}-\left(\frac{\sigma}{R}\right)^6\right], \quad \text{(A12)}$$

with

$$R=|\mathbf{r}-\mathbf{r}'|. \quad \text{(A13)}$$

Here σ and ϵ stand for σ_{LJ} and ϵ_{LJ}, respectively. In this case one can follow the same procedure as that utilized to calculate the ''coarse-grained density'' terms. As before there are three different domains of r to be considered. At $r=0$ the Hartree potential reads

$$V_H^{\mathrm{LJ\,Scr}}(r=0)=\frac{4\pi}{h_{\mathrm{OP}}^4}V_l^{\mathrm{OP}}(h_{\mathrm{OP}})\int_0^{h_{\mathrm{OP}}} r'^6 dr'\rho(r') + 16\pi\epsilon\int_{h_{\mathrm{OP}}}^{\infty} r'^2 dr'\rho(r')\left[\left(\frac{\sigma}{r'}\right)^{12}-\left(\frac{\sigma}{r'}\right)^6\right]. \quad \text{(A14)}$$

For $0<r<h_{\mathrm{OP}}$ the integral over r' becomes

$$V_H^{\mathrm{LJ\,Scr}}(r)=\frac{\pi h_{\mathrm{OP}}^2}{3r}V_l^{\mathrm{OP}}(h_{\mathrm{OP}})\Bigg\{\int_0^{h_{\mathrm{OP}}-r} r'dr'\rho(r')\times\left[\left(\frac{r+r'}{h_{\mathrm{OP}}}\right)^6-\left(\frac{r-r'}{h_{\mathrm{OP}}}\right)^6\right]+\int_{h_{\mathrm{OP}}-r}^{r+h_{\mathrm{OP}}} r'dr'\rho(r')\times\left[1-\left(\frac{r-r'}{h_{\mathrm{OP}}}\right)^6\right]\Bigg\}+\frac{4\pi\epsilon\sigma^2}{r}\int_{h_{\mathrm{OP}}-r}^{r+h_{\mathrm{OP}}} r'dr'\rho(r')\times\left\{\frac{1}{5}\left[\left(\frac{\sigma}{h_{\mathrm{OP}}}\right)^{10}-\left(\frac{\sigma}{r+r'}\right)^{10}\right]-\frac{1}{2}\left[\left(\frac{\sigma}{h_{\mathrm{OP}}}\right)^4-\left(\frac{\sigma}{r+r'}\right)^4\right]\right\}+\frac{4\pi\epsilon\sigma^2}{r}\int_{r+h_{\mathrm{OP}}}^{\infty} r'dr'\rho(r')\times\left\{\frac{1}{5}\left[\left(\frac{\sigma}{r-r'}\right)^{10}-\left(\frac{\sigma}{r+r'}\right)^{10}\right]-\frac{1}{2}\left[\left(\frac{\sigma}{r-r'}\right)^4-\left(\frac{\sigma}{r+r'}\right)^4\right]\right\}. \tag{A15}$$

Finally, for $r\geqslant h_{\mathrm{OP}}$ one gets

$$V_H^{\mathrm{LJ\,Scr}}(r)=\frac{\pi h_{\mathrm{OP}}^2}{3r}V_l^{\mathrm{OP}}(h_{\mathrm{OP}})\int_{r-h_{\mathrm{OP}}}^{r+h_{\mathrm{OP}}}\rho(r')\times\left[1-\left(\frac{r-r'}{h_{\mathrm{OP}}}\right)^6\right]r'dr'+\frac{4\pi\epsilon\sigma^2}{r}\Bigg\{\int_0^{r-h_{\mathrm{OP}}}+\int_{r+h_{\mathrm{OP}}}^{\infty}\Bigg\}r'dr'\rho(r')\left\{\frac{1}{5}\left[\left(\frac{\sigma}{r-r'}\right)^{10}-\left(\frac{\sigma}{r+r'}\right)^{10}\right]-\frac{1}{2}\left[\left(\frac{\sigma}{r-r'}\right)^4-\left(\frac{\sigma}{r+r'}\right)^4\right]\right\}+\frac{4\pi\epsilon\sigma^2}{r}\int_{r-h_{\mathrm{OP}}}^{r+h_{\mathrm{OP}}} r'dr'\rho(r')\left\{\frac{1}{5}\left[\left(\frac{\sigma}{h_{\mathrm{OP}}}\right)^{10}-\left(\frac{\sigma}{r+r'}\right)^{10}\right]-\frac{1}{2}\left[\left(\frac{\sigma}{h_{\mathrm{OP}}}\right)^4-\left(\frac{\sigma}{r+r'}\right)^4\right]\right\}. \tag{A16}$$

APPENDIX B: SIMPLE MODEL I

Starting from Eqs. (4.43) and (4.44), after imposing continuity of functions and derivatives one gets

$$\rho(z_\ell)=\rho_c\left[1-\frac{4(z_\ell-z_0)}{5W}\right]=\frac{\rho_c}{\alpha}, \tag{B1}$$

and

$$\left[\frac{d\rho(z)}{dz}\right]_{z=z_\ell}=-\frac{4\rho_c}{5W}=-\frac{2B\rho_c}{\alpha}. \tag{B2}$$

These conditions lead to

$$\alpha=\frac{5}{2}BW, \tag{B3}$$

and

$$z_\ell-z_0=\frac{5}{4}W-\frac{1}{2B}=\frac{9}{8}W+\left(\frac{W}{8}-\frac{1}{2B}\right). \tag{B4}$$

Since for large slabs one expects $W>4/B\simeq 3.7$ Å, then $z_\ell-z_0$ would be larger than $9W/8$, ensuring $\rho(z_\ell)<\rho_c/10$, which in turn would support the consistency of the adopted law for the falloff and the definition of the thickness.

For the evaluation of the derivative one may use the relation

$$\frac{d\sqrt{\rho(z)}}{dz}=\frac{1}{2\sqrt{\rho(z)}}\frac{d\rho(z)}{dz}. \tag{B5}$$

Now, the integral of Eq. (4.42) may be split into two parts,

$$\sigma_A=\left\{\int_{z_0}^{z_\ell}+\int_{z_\ell}^{\infty}\right\}dz\left[\frac{\hbar^2}{4m}\frac{1}{\rho(z)}+2d_4\right]\left[\frac{d\rho(z)}{dz}\right]^2, \tag{B6}$$

which leads to

$$\sigma_A=\frac{\rho_c}{5W}\left\{\frac{\hbar^2}{m}\left[1+\ln\left(\frac{5}{2}BW\right)\right]+8d_4\rho_c\left[1-\frac{1}{5BW}\right]\right\}. \tag{B7}$$

It is possible to verify that for the expected values of W there is an important cancellation between terms carrying the product BW. Hence, Eq. (B7) may be reduced to

$$\sigma_A\simeq\frac{\rho_c}{5W}\left(\frac{\hbar^2}{m}+8d_4\rho_c\right). \tag{B8}$$

APPENDIX C: SIMPLE MODEL II

The evaluation of the normalization condition yields

$$N=\Omega_D\rho_c\frac{[R_s+(1-\beta)W]^{D+1}-[R_s-\beta W]^{D+1}}{D(D+1)L^{D-3}W}, \tag{C1}$$

with $\Omega_{D=1}=2$, $\Omega_{D=2}=2\pi$, and $\Omega_{D=3}=4\pi$. In the case $D=1$ the "sharp radius" R_s stands for z_s. The parameter β becomes

(i) for the planar geometry

$$\beta=\frac{1}{2}, \tag{C2}$$

(ii) for cylinders

$$\beta=\frac{1}{2}+\frac{R_s}{W}-\sqrt{\left(\frac{R_s}{W}\right)^2-\frac{1}{12}}, \tag{C3}$$

(iii) and for spheres

$$\beta=\frac{1}{2}+\frac{R_s}{W}-\frac{1}{2^{1/3}}\left[\left(\frac{R_s}{W}\right)^3+\sqrt{\left(\frac{R_s}{W}\right)^6+\frac{1}{2\times 6^3}}\right]^{1/3}+\frac{2^{1/3}}{12}\left[\left(\frac{R_s}{W}\right)^3+\sqrt{\left(\frac{R_s}{W}\right)^6+\frac{1}{2\times 6^3}}\right]^{-1/3}. \quad \text{(C4)}$$

For instance, the ground-state energy for cylindric geometry reads

$$e=e_B+2\pi n_\lambda^{-1}\left\{\frac{1}{2}e_B\beta W(-2R_s+\beta W)\rho_c+\left(\frac{1}{2}+\frac{R_s}{W}-\beta\right)\times\left(\frac{\hbar^2}{2m}+d_4\rho_c\right)\rho_c+\frac{1}{6}W^2\rho_c^2\left[b_4\left(\frac{1}{4}+\frac{R_s}{W}-\beta\right)+\frac{3c_4}{\gamma_4+3}\left(\frac{1}{\gamma_4+4}+\frac{R_s}{W}-\beta\right)\rho_c\right]\right\}. \quad \text{(C5)}$$

Here ρ_c and R_s are functions of ϵ given by Eqs. (4.1) and (4.7), respectively.

*Also at the Carrera del Investigador Científico of the Consejo Nacional de Investigaciones Científicas y Técnicas, Av. Rivadavia 1917, RA-1033 Buenos Aires, Argentina.

†Also at the Comisión de Investigaciones Científicas de la Prov. de Buenos Aires, Calle 526 entre 10 y 11, RA-1900 La Plata, Argentina.

[1] D.O. Edwards and W.F. Saam, in *Progress in Low Temperature Physics*, edited by D.F. Brewer (North-Holland, Amsterdam, 1978), Vol. 7A, Chap. 4.

[2] D.V. Osborne, J. Phys.: Condens. Matter **1**, 289 (1989).

[3] L.B. Lurio, T.A. Rabedeau, P.S. Pershan, I.F. Silvera, M. Deutsch, S.D. Kosowsky, and B.M. Ocko, Phys. Rev. Lett. **68**, 2628 (1992); Phys. Rev. B **48**, 9644 (1993).

[4] J. Harms, J.P. Toennies, and F. Dalfovo, Phys. Rev. B **58**, 3341 (1998).

[5] L. Szybisz, Eur. Phys. J. B **14**, 733 (2000).

[6] D.E. Galli and L. Reatto, J. Phys.: Condens. Matter **12**, 6009 (2000).

[7] K. Penanen, M. Fukuto, R.K. Heilmann, I.F. Silvera, and P.S. Pershan, Phys. Rev. B **62**, 9621 (2000).

[8] H.M. Guo, D.O. Edwards, R.E. Sarwinski, and J.T. Tough, Phys. Rev. Lett. **27**, 1259 (1971).

[9] M. Iino, M. Suzuki, and A.J. Ikushima, J. Low Temp. Phys. **61**, 155 (1985).

[10] P. Roche, G. Deville, N.J. Appleyard, and F.I.B. Williams, J. Low Temp. Phys. **106**, 565 (1997).

[11] V.R. Pandharipande, J.G. Zabolitzky, S.C. Pieper, R.B. Wiringa, and U. Helmbrecht, Phys. Rev. Lett. **50**, 1676 (1983); V.R. Pandharipande, S.C. Pieper, and R.B. Wiringa, Phys. Rev. B **34**, 4571 (1986).

[12] J.L. Vallés and K.E. Schmidt, Phys. Rev. B **38**, 2879 (1988).

[13] S. Stringari and J. Treiner, J. Chem. Phys. **87**, 5021 (1987).

[14] G. Stan and M.W. Cole, Surf. Sci. **395**, 280 (1998).

[15] M.W. Cole, V.H. Crespi, G. Stan, C. Ebner, J.M. Hartman, S. Morini, and M. Boninsegni, Phys. Rev. Lett. **84**, 3883 (2000).

[16] S.M. Gatica, G. Stan, M.M. Calbi, J.K. Johnson, and M.W. Cole, J. Low Temp. Phys. **120**, 337 (2000).

[17] L. Szybisz, Physica A **283**, 193 (2000).

[18] L. Szybisz and S.M. Gatica, Phys. Rev. B **64**, 224523 (2001).

[19] M.P. Lilly and R.B. Hallock, Phys. Rev. B **63**, 174503 (2001).

[20] L. Szybisz and I. Urrutia, Phys. Rev. E **66**, 051201 (2002).

[21] S. Stringari and J. Treiner, Phys. Rev. B **36**, 8369 (1987).

[22] J. Dupont-Roc, M. Himbert, N. Pavloff, and J. Treiner, J. Low Temp. Phys. **81**, 31 (1990).

[23] P. Ring and P. Schuck, *The Nuclear Many-body Problem* (Springer, Berlin, 1980).

[24] S. Stringari, Phys. Lett. **106A**, 267 (1984); **107A**, 36 (1985).

[25] F. Dalfovo, A. Lastri, L. Pricaupenko, S. Stringari, and J. Treiner, Phys. Rev. B **52**, 1193 (1995).

[26] J. de Boer and A. Michels, Physica (Amsterdam) **6**, 945 (1938).

[27] E. Cheng, M.W. Cole, W.F. Saam, and J. Treiner, Phys. Rev. B **46**, 13 967 (1992).

[28] M. Barranco and E.S. Hernández, Phys. Rev. B **49**, 12 078 (1994).

[29] K.W. Ford and J.G. Wills, Phys. Rev. **185**, 1429 (1969).

[30] J. Treiner, W.D. Myers, W.J. Swiatecki, and M.S. Weiss, Nucl. Phys. A **452**, 93 (1986).

[31] J. Treiner and H. Krivine, Ann. Phys. (N.Y.) **170**, 406 (1986).

[32] J.S. Rowlinson and B. Widom, *Molecular Theory of Capillarity* (Clarendon, Oxford, 1982).

[33] A. Chizmeshya, M.W. Cole, and E. Zaremba, J. Low Temp. Phys. **110**, 677 (1998).

[34] L. Szybisz, Phys. Rev. B **62**, 12 381 (2000).

[35] In this case, results for the thickness are plotted at the abscissa $\Delta e=e-e_B$ corresponding to free planar films of $n_c=0.34$ Å^{-2}, but data are slightly shifted to be distinguished.

[36] D.O. Edwards and P.P. Fatouros, Phys. Rev. B **17**, 2147 (1978).